ACS OMEGA

http://pubs.acs.org/journal/acsodf

Article

Experimental Investigation and Time Effect on the Anticorrosion and Microstructural Properties of Zinc Flake Nickel−Phosphorus Coating Electrodeposited on Mild Steel

Ojo Sunday Isaac Fayomi,* Sode Adedamola Ayodeji, Oluranti Agboola, Kunle Michael Oluwasegun, and Mojisola Olubunmi Nkiko

Cite This: *ACS Omega* 2021, 6, 11139−11143

Read Online

ACCESS | Metrics & More | Article Recommendations

ABSTRACT: In this work, the potential of $ZnSO_4{\cdot}7H_2O$ in NiP sulphate electrolyte deposited on mild steel under constant optimum pH of 5, current density of 1 A/cm^2, stirring rate of 200 rpm, and varying time parameter between 10, 15, 20, and 25 min were studied using the electrodeposition method. The microstructure properties and corrosion resistance characteristics were analyzed using a scanning electron microscope enhanced with an energy-dispersive spectroscope and potentiodynamic polarization apparatus, respectively. The codeposited was subjected to different media test rig of 0.5 M H_2SO_4 and 3.5% NaCl to examine the susceptibility effect. The results pointed out that there is a stable mass weight gain as the time increases, which facilitates the formation of dispersed crystal build-up and homogeneous NiPZn content within the interface. A remarkable corrosion property was also noticed with deposits of highest time effect, which is invariably a factor of solid bonding seen at the surface lattice.

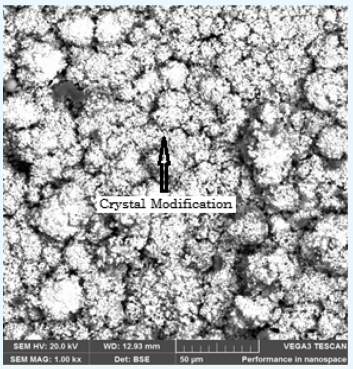

1. INTRODUCTION

Mild-steel accessibility and durability in many engineering services concerning cost, availability, formability, and satisfactory mechanical behavior cannot be overemphasized.[1−3] Thus, its functionality and electrochemical retardant are of great concern in application because of massive deterioration, pitting evolution, instability at high temperature, and low structural vulnerability.[4] However, in special conditions and services, a structural application involving steel such as automobile, manufacturing plant, bridges, petrochemical highways, and so forth is vulnerable to the limitation in hardness and corrosion fallout.[5−8]

Corrosion problems can be detrimental and consequential leading to leakage and contamination.[9] The surface modification becomes a practical application in addressing these catastrophes.[10] Modification of the interface of substrate or surfaces is an act of changing or altering expose layers of metal to provide unique properties.[11] This alteration gives underlayer material exclusive coverage by modifying the physical, mechanical, and corrosion behavior.[12] Research and development by many researchers involving the development of a coating that will enhance the surface layer of metallic materials, especially carbon steel, are numerous.[13−15] Properties' evolution of steel substrate for effective corrosion control using zinc- and nickel-based coating is on the increase.[16] The reason not far fetches from the protective oxide formation that extensively provides passivation potential at the steel interface.[17] A stringent application that required a highly protective coating, fabricated with ceramics and metal oxide composite coating, has been demonstrated to be a good choice. For instance, a report by various investigators accounts for a better alternative of a composite additive such as Al_2O_3, SnO_2, TiO_2, NiO, Y_2O_3, Cr_2O_3, and SiO_2, which support anomalous abundant deposition.[18−20]

With nickel−phosphate deposition on steel, nonhomogeneous coating with lustrous hexagonal flakes was often characterized with the deposit because of the absence of some solute additives leading to the limitation in corrosion and structural responses. It is a well-known fact that nickel−phosphate provides affinity to the adsorbed ceramic composite, metal oxide nanoparticle, and crystallites with inert potential. In dual-anode electrolytic deposition, it is hard to control the crystal formation without the understanding of both framework and process parameters. For other desired specific material properties, crystals of zinc were induced in NiP electrolyte with a variation of time-dependent in an attempt to develop stable structural, mechanical, and corrosion protection.

Received: April 22, 2020
Accepted: July 20, 2020
Published: April 21, 2021

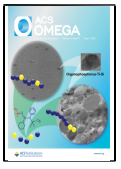

https://doi.org/10.1021/acsomega.0c01861
ACS Omega 2021, 6, 11139−11143

Table 1. Compositional Value in Weight Percent of Unplated Mild Steel

element	S	Mn	Si	Ni	Al	P	C	Fe
composition (%)	0.02	0.15	0.016	0.01	0.01	0.01	0.032	balance

2. EXPERIMENTAL METHODS

2.1. Sample Preparation. The obtained mild-steel plate used in the research was divided into equal portion of 40 mm × 40 mm × 2 mm with the aid of Struers Discotom precision cutter at 600 rpm. The steel plate purchased from a metal-processing vendor in Ota, Nigeria, was analyzed accordingly. The percentage nominal weight composition of the mild-steel substrate is presented in Table 1. The preparation of the mild-steel surface follows precision process of surface preparation technology for degreasing and descaling by ref 7. All chemical reagents used are of Analar grade and conformed to standard for the electrodeposition route. The bath formulation was prepared 24 h ahead for proper dissolution and the content free from agglomeration.[10]

2.2. Electrodeposition Bath and Formulation. All chemicals used in this study were obtained and supplied to Surface Engineering Research Laboratory, Covenant University from Sigma-Aldrich, USA. $NiSO_4{\cdot}6H_2O$, $ZnSO_4{\cdot}7H_2O$, and $NaH_2PO_2{\cdot}H_2O$ salt were obtained in powder form. $NiSO_4{\cdot}6H_2O$, which is the base salt, has a density of 2.07 g/cm^3 and solubility in water of 77.5 g/mL at 30 °C. $ZnSO_4{\cdot}7H_2O$ is a hydrated crystal that crystallizes in orthorhombic nature with a density of 3.31 g/cm^3, dissolving freely in water at 280 °C, and a molar mass of 287.54. The weight percentage of the $ZnSO_4{\cdot}7H_2O$, is at a constant concentration of 30 g/L. The bath formulation was obtained by dissolving 30 g of $NiSO_4{\cdot}6H_2O$, 30 g of $ZnSO_4{\cdot}7H_2O$, 33 g of $NaH_2PO_2{\cdot}H_2O$, 60 g of $C_6H_5{\cdot}Na_3O_7{\cdot}2H_2O$, 25 g of $(NH_4)_2SO_4$, 10 g of H_3BO_3, and 10 g of thiourea in 1 L of deionized water at pH of 5. The bath was allowed to dissolve appropriately after leaving it for 24 h. Most of the admixtures constituting the bath formulation are for quick conductivity of cation, brightener, buffers, and refiners.

2.3. Design of Experiment and Process Setup. The electrodeposition setup used is self-assembled, being a process that utilizes electric current to cause a reduction of dissolved metal ions to take position forming a thin layer of film on an electrode. Requirements for electroplating are a power supply in the form of a DC rectifier, an electrolyte solution, a cathode, and an anode. Other components necessary to foster easier use and better coating include a nonconductive container (conical glass flasks), jumper cables with alligator clips, a stirrer, and a heater. The mild-steel sample was submerged in the electrolyte developed through a self-developed bath combination and connected as the cathode to the setup. At the same time, two large nickel bars were placed equidistant from the mild steel in the electrolyte also in the conical flask, connected as the anode. Electrons flow from the anode to cathode through the electrolyte, and the flow of electrons is dependent on the potential difference between the terminals. A sulphate electrolyte with nickel- and zinc-based salt was used in this study. The constituents of each bath are prepared by measuring in grams stated earlier with the OHAUS Pioneer PA214 electrical analytical weighing balance. After the measurement, the compounds are put into a container, distilled water is poured into the container, and the contents are mixed and allowed to dissolve. The bath is prepared and placed on a hot stirrer with the temperature set to 40 °C and stirring speed at 250 rpm. The electrolytic cell setup is prepared by placing two nickel anodes and a copper wiring connecting the anodes together and the beam support made of copper for the cathode, which is the mild steel. The setup was connected to a DC rectifier, with the anodes connected to the positive terminal and the cathode connected to the negative terminal, which follows the standard of design by ref 5. The coating occurred at a potential difference of 2 V and current density of 1 A/cm^2 at 10, 15, 20, and 25 min as projected in the design of the experiment. The components of the bath were changed after each time cycle in the presence of $ZnSO_4{\cdot}7H_2O$. The coated samples after successful deposition were air-dried and stored in a cool and dry place (Table 2).

Table 2. Experimental Design of Study for Electrodeposition of Ni−P−Zn

sample coating	time (min)
Ni−P−Zn	10
Ni−P−Zn	15
Ni−P−Zn	20
Ni−P−Zn	25

2.4. Structural Analysis of Codeposited Mild Steel. All developed codeposited coatings and starting materials were examined using scanning electron microscopy (SEM) and energy-dispersive spectroscopy (EDS). EGA 3, TESCAN model SEM checked the arrangement and deposits crystals of the electrodeposited mild steel.

2.5. Corrosion Analysis. Investigation on the corrosion properties of electrodeposited coatings under different particle weight compositions was studied using linear sweep voltammetry with open-circuit potential. The produced coating samples were subjected to acidic and sea-like (salty) environments at an ambient temperature of (27 ± 1 °C). A three conventional electrode cell consisting of the reference electrode, working electrode, and counter electrode with a beaker filled with 100 mL of electrolyte was used. With the mild steel as the working electrode, silver chloride as the reference electrode, and graphite rod as the counter electrode, the configuration was connected to AUTO LAB PGSTAT 101 Metrohm. The Tafel plot was attained within −1.5 and +1.5 V and a scan rate of 0.0012 V/s. The assessment is in par with procedure studied by ref 6 at several concentrations and while changing the temperature of the system.

$$\mathrm{IE}\ (\%) = \frac{(J_{\mathrm{corr}})_a - (J_{\mathrm{corr}})_p}{(J_{\mathrm{corr}})_a} \times 100 \quad (1)$$

where $(I_{\mathrm{corr}})_a$ and $(I_{\mathrm{corr}})_p$ represent the corrosion density (A cm^{-2}) in the absence and presence of the particulate, respectively.

3. RESULTS AND DISCUSSION

3.1. Electrodeposition Results. In Table 3, a variation of time on the progression of electrolytic deposition at different coating matrices to determine adsorbed particle's physical responses and its effectiveness was studied. The distribution of all electrodeposited coatings in terms of weight gain and

https://doi.org/10.1021/acsomega.0c01861
ACS Omega 2021, 6, 11139−11143

Table 3. Electrodeposition Parameters and Results for Ni−P−Zn Coating

sample coating	time (min)	weight gain (g)	coating per unit area (mg/mm^2)
Ni−Zn−P	10	0.0832	0.034667
Ni−Zn−P	15	0.1464	0.061000
Ni−Zn−P	20	0.1806	0.075250
Ni−Zn−P	25	0.2622	0.109250

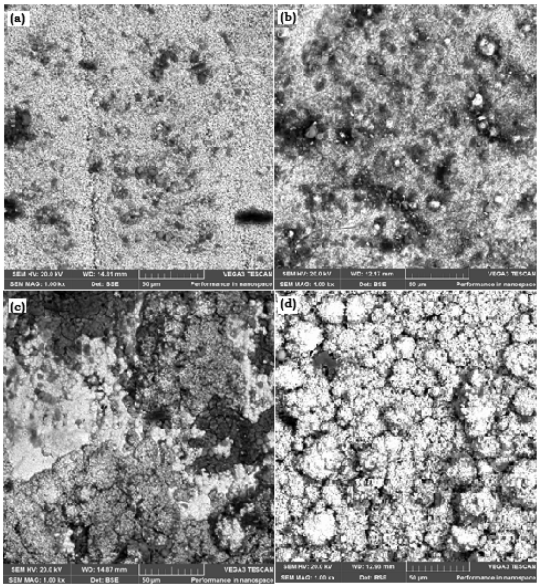

Figure 1. SEM crystal evolution of codeposition of the Ni−P−Zn mild-steel surface at ×1000 magnification: (a) 10 (b) 15 (c) 20 and (d) 25 min.

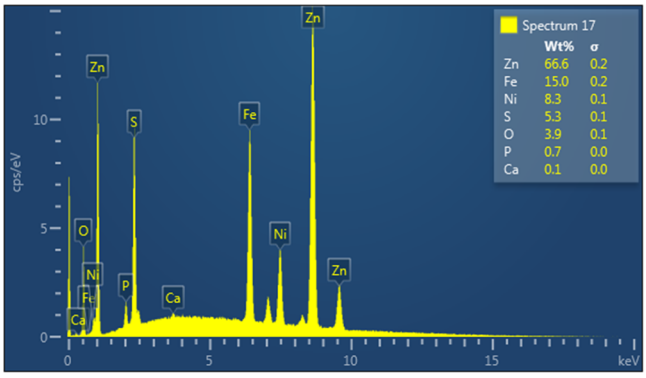

Figure 2. EDS elemental quantification of Ni−P−Zn deposited mild-steel surface at 25 min.

coating per unit area as the time increase is revealed in Table 3. It is reasonable to note that the weight gain of the NiP−Zn-25 min codeposition increases significantly with an increase in time with 0.2622 g to 0.109250 A/m^2 for weight gained and coating per unit area, respectively. Noticeably, with NiP−Zn-20 min coating deposited possess 0.0832 g to 0.034667 A/m^2 as correspondence weight gained and layer per unit area. It was found that surface coverage build-up of all fabricated coatings has an excellent response to the time difference. It is also essential to ascertain that the influence of the deposition parameter can be seen to determine the degree of coating thin film formed on a mild-steel substrate. With this considerable increase in weight gain, one can see linearity in the formation

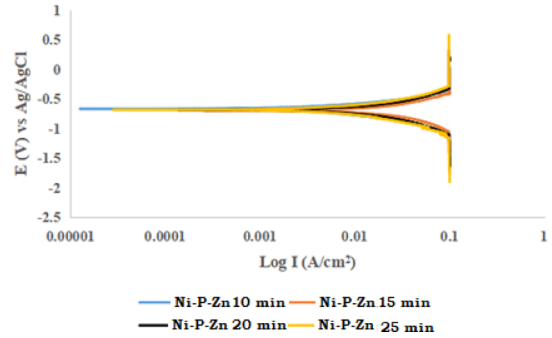

Figure 3. Potentiodynamic polarization curve for codeposited Ni−P−Zn at different time variations in 0.5 M H_2SO_4.

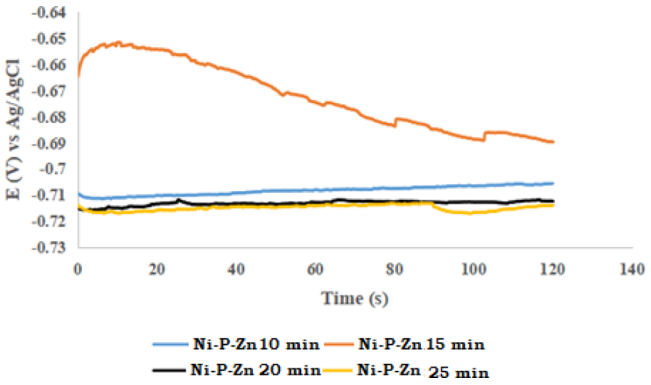

Figure 4. Open-circuit potential curve for codeposited Ni−P−Zn at different time variations in 0.5 M H_2SO_4.

of coating thickness. This property between the linear relationship of time of deposition and physical characteristics is reported by ref 8.

The SEM structure of Ni−Zn−P is presented Figure 1a−d under difference in time of deposition from ranging from 10 to 25 min. The electrodeposited coating was done at 1.00k× magnifications, with an acceleration voltage of 20 kV; working distance 50 μm. The sample with 20 min coating, as presented in Figure 1a, shows significant deposits and refine precipitations from the induced salt, thus the alteration in the morphology with smaller oxide film.[2−5] On the other hand, the time difference was appreciated with beneficial zinc crystal diffuse into the nickel−phosphorus interstitial space through the electrophoresis mechanism. More dispatched zinc and amorphous structure with circular, fibrous stable flake film was deposited, as shown in Figure 1b, when the time was increased to 15 min. The grain and precipitated constituent account for the more distinctive phase at the interface of the mild steel. This marginal improvement is obviously as a result of possible inherent complexes that simultaneously interact and align with the condition for perfect dispersion.[4] Remarkably, morphological changes often provide evidence of particle-hardening content.[5] This formative change in the structure was seen with a deposited coating of 20 min with zinc ion solidly within the atomic radii of NiP pores. However, coating stability and perfect bounding with appreciable embedded zinc solute solution were noticed with a coating having a deposition time of 25 min. It can also be said that crystal evolution is free from stress and depressed pores because of the interfacial responses of the time deviation.

After SEM study, the EDX pattern for elemental constituent was examined and presented, as shown in Figure 2, for Ni−

https://doi.org/10.1021/acsomega.0c01861
ACS Omega 2021, 6, 11139−11143

Table 4. Potentiodynamic Polarization Table for Codeposited Ni−P−Zn at Different Time Variations in 0.5 M H_2SO_4

sample label	E_{corr} (V)	J_{corr} (A/cm^2)	corrosion rate (mm/year)	polarization resistance (Ω)
Ni−P−Zn-10 min	−0.74521	0.0038031	3.7321	62.234
Ni−P−Zn-15 min	−0.73671	0.0036562	1.4211	65.771
Ni−P−Zn-20 min	−0.72512	0.0029845	1.2321	72.245
Ni−P−Zn-25 min	−0.72212	0.0029221	1.2210	85.123

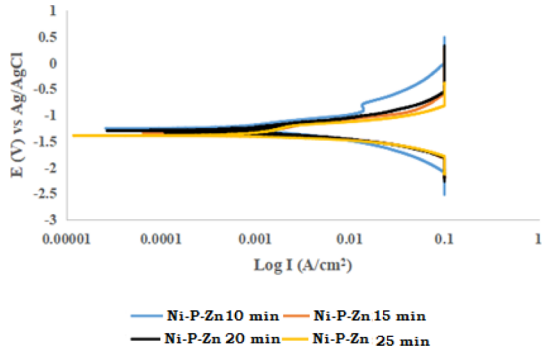

Figure 5. Potentiodynamic polarization curve for codeposited Ni−P−Zn at different time variations in 3.5% NaCl.

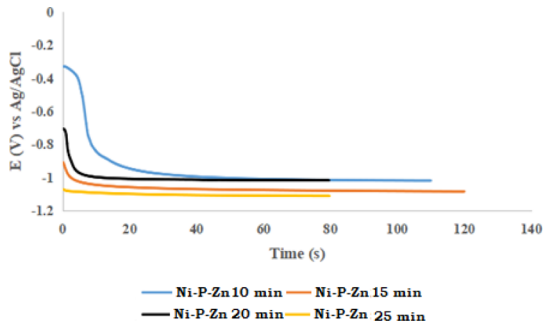

Figure 6. Open-circuit potential curve codeposited Ni−P−Zn at different time variations in 3.5% NaCl.

Zn−P coating at 25 min. The second-phase particle containing the presence of zinc, nickel, phosphorus, and oxygen was observed. The zinc content has the highest weight deposit, with 66.6% providing a stable evolution. Other elemental deposited particle also acts as dispersive nucleation promoting fibrous flakes.

Figures 3 and 4 show the potentiodynamic polarization and open-circuit potential plots of deposited coating done on Ni−P−Zn by the electrodeposition route from 10 to 25 min. The effect of potential−current density change was examined in 0.5 M H_2SO_4 for all coating alloys. The obtained result, as shown in Table 4, indicates that activities of a developed alloy of NiPZn alloy for 20 and 25 min generally show passive surface responses. The corrosion rate decreases with an increase in deposition time. It is critical at this stage to establish that the influence of interfacial atomic constitutes provided the stable orientation of the thin flakes. Meanwhile, the NiPZn-10 min

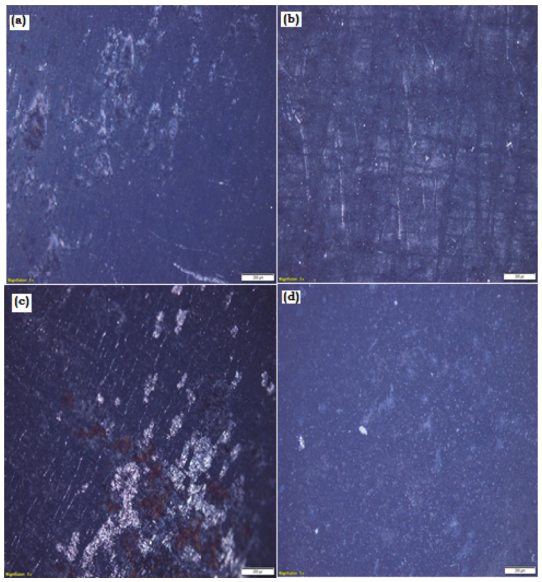

Figure 7. Morphology of corroded Ni−P−Zn deposited on the mild-steel surface at ×5 magnification: (a) 10, (b) 15, (c) 20, and (d) 25 min.

coated on mild steel shows a polarization resistance of 62.234 Ω, the corrosion rate of 3.7321 mm/y, and potential corrosion effect of 0.74521 V. With NiP−Zn-25 min coating, the effect of extended transfer time mechanism was seen, with a strong bonding polarization resistance of 85.123 Ω, corrosion rate of 1.2210 mm/yr, and corrosion potential of −0.72212 V. It should be noted that nucleation at the interface was perfect leading to barriers of SO_4^{2+} and Fe^{2+} species, which are responsible for accelerating the corrosion process.

There is a level of compliance and similar progression, as demonstrated in Figures 5 and 6, on the susceptibility of the electrodeposited coatings in 3.65% NaCl solution. From Table 5, Tafel extrapolation data indicated that there is a shift in the potential to the more potential region as the time of deposition increases within the deposition matrix. The presence of the adsorbed second phase metal ion influences the anodic and cathodic branch from the Tafel curve. NiP−Zn-25 min has a polarization resistance of 54.791 Ω, the corrosion rate of 4.6210 mm/y, and corrosion potential effect of −1.42321 V. The corrosion properties with 10 min coating deposited has a corrosion polarization resistance of 79.234 Ω, the corrosion rate of 1.4321 mm/y, and corrosion potential effect of

Table 5. Potentiodynamic Polarization Table for Codeposited Ni−P−Zn at Different Time Variations in 3.5% NaCl

sample label	E_{corr} (V)	J_{corr} (A/cm^2)	corrosion rate (mm/year)	polarization resistance (Ω)
Ni−P−Zn-10 min	−1.22423	0.009807	1.4321	79.234
Ni−P−Zn-15 min	−1.23111.	0.009901	1.8543	75.771
Ni−P−Zn-20 min	−1.36522	0.009976	2.1456	62.118
Ni−P−Zn-25 min	−1.42321	0.012134	4.6210	54.791

https://doi.org/10.1021/acsomega.0c01861
ACS Omega 2021, 6, 11139−11143

−1.22423. This observation implies that there is more Fe^{2+} ion dissolution with chloride influence compare to when the sulphate ion was induced.

The as-corroded samples of all deposited coatings in their time variation are presented in Figure 7a−d. Generally, all the deposited coatings show a more adhered and stable effect after corrosion interference except for Ni−P−Zn-20 min, which shows some pitting, excessive scale, and corrosion product. It is expected that a good bounding interface will slow down the interference of halide ions that could cause vulnerability within the interface, as reported by ref.[5,7] In conclusion, the build-up of the clusters demonstrated at the structural image has an essential influence on the susceptibility of the developed coatings.

4. CONCLUSIONS

A typical simple and cost-effective electrodeposition method was used to fabricate Ni−P−Zn coating for marine applications. An appropriate processed condition was identified after optimization. A precipitation and modified zinc content that is uniformly distributed as a phase constituent on the NiP matrix was obtained after material characterization showing porous-free hybrid matrices. From the electrochemical study, higher corrosion resistance properties were attained as the time of deposition increases. Significantly, a predominant refine crystal orientation on the morphology was noticed after corrosion with the typical flake-like structure in the thin film attained. It is worth mentioning to say that coatings possess stress, porosity, and a crack-free layer at the optimum time.

AUTHOR INFORMATION

Corresponding Author

Ojo Sunday Isaac Fayomi − *Department of Mechanical and Biomedical Engineering, Bells University of Technology, Ota, Nigeria;* orcid.org/0000-0001-9023-2371; Phone: +2348036886783; Email: Ojosundayfayomi3@gmail.com, osfayomi@bellsuniversity.edu.ng

Authors

Sode Adedamola Ayodeji − *Department of Mechanical Engineering, Covenant University, Ota, Nigeria*

Oluranti Agboola − *Department of Chemical Engineering, Covenant University, Ota, Nigeria*

Kunle Michael Oluwasegun − *Department of Mechanical and Manufacturing Engineering, University of Manitoba, Winnipeg, Manitoba, Canada*

Mojisola Olubunmi Nkiko − *Department of Physical and Chemical Sciences, Elizade University, Ilara-Mokin, Nigeria*

Complete contact information is available at: https://pubs.acs.org/10.1021/acsomega.0c01861

Notes

The authors declare no competing financial interest.

ACKNOWLEDGMENTS

The authors appreciate gracefully Surface Engineering Research Laboratory, Bells University of Technology, and Covenant University for equipment usage.

REFERENCES

(1) Ahmad, Y. H.; Mohamed, A. M. A. Electrodeposition of nanostructured nickel-ceramic composite coatings: A review. *Int. J. Electrochem. Sci.* **2014**, *9*, 1942−1963.

(2) Akande, I. G.; Oluwole, O. O.; Fayomi, O. S. I. Optimizing the defensive characteristics of mild steel via the electrodeposition of Zn-Si_3N_4 reinforcing particles. *Def. Technol.* **2019**, *15*, 526−532.

(3) Koch, G. H.; Brongers, M. P.; Thompson, N. G., Virmani, Y. P.; Payer, J. H. *Corrosion Cost and Preventive Strategies in the United States*; Federal Highway Administration, 2002; Vol. *1*, pp 156−164.

(4) Jackson, M.; Deocampo, D.; Marra, F.; Scheetz, B. Mid-Pleistocene pozzolanic volcanic ash in ancient Roman concretes. *Geoarchaeology* **2010**, *25*, 36−74.

(5) Anawe, P. A. L.; Fayomi, O. S. I.; Popoola, A. P. I. Results in physics investigation of microstructural and physical characteristics of nano composite tin oxide-doped Al^{3+} in Zn^{2+} based composite coating by DAECD technique. *Results Phys.* **2017**, *7*, 777−788.

(6) Ashby, M. F. Engineering Materials 1: An Introduction to Properties, Applications and Design. *Materials Selection in Mechanical Design*; Butterworth-Heinemann, 2011; Vol. *1*, pp 1−464.

(7) Aydoğdu, G. H.; Aydinol, M. K. Determination of susceptibility to intergranular corrosion and electrochemical reactivation behaviour of AISI 316L type stainless steel. *Corr Sci* **2006**, *48*, 3565−3583.

(8) House, K.; Sernetz, F.; Dymock, D.; Sandy, J. R.; Ireland, A. J. Corrosion of orthodontic appliances—should we care? *Amer. J. ortho. and dento. ortho.* **2008**, *133*, 584−592.

(9) Inoue, R.; Arai, Y.; Kubota, Y.; Kogo, Y.; Goto, K. Oxidation of ZrB_2 and its composites: a review. *J. Mater. Sci.* **2018**, *53*, 14885−14906.

(10) Ayoola, A. A.; Fayomi, O. S. I.; Ogunkanmbi, S. O. Data in brief data on inhibitive performance of chloraphenicol drug on A315 mild steel in acidic medium. *Data in Brief* **2018**, *19*, 804−809.

(11) Jirarungsatian, C.; Prateepasen, A. Pitting and uniform corrosion source recognition using acoustic emission parameters. *Corro Sci* **2010**, *52*, 187−197.

(12) Kallappa, D.; Venkatarangaiah, V. T. Synthesis of CeO_2 doped ZnO nanoparticles and their application in Zn-composite coating on mild steel. *Arabian J. Chem.* **2020**, *13*, 2309−2317.

(13) Krishnan, K. H.; John, S.; Srinivasan, K. N.; Praveen, J.; Ganesan, M.; Kavimani, P. M. An overall aspect of electroless Ni-P depositions — A Review Article. *Metal. and Mat. Trans. A.* **2006**, *37*, 1917−1926.

(14) Equbal, A.; Dixit, N. K.; Sood, A. K. Electroless plating on plastic. *Int. J. Appl. Sci. Eng. Res.* **2013**, *8*, 12−18.

(15) Gao, W.; Cao, D.; Jin, Y.; Zhou, X.; Cheng, G.; Wang, Y. Microstructure and properties of Cu-Sn-Zn-TiO_2 nano-composite coatings on mild steel. *Surf. Coat. Technol.* **2018**, *350*, 801−806.

(16) Laudisio, G.; Seipel, B.; Ruffini, A.; Nickel, K. G. Corrosion behavior of Si_3N_4−TiN composite in sulphuric acid. *Corros. Sci.* **2005**, *47*, 1666−1677.

(17) Li, B.; Li, D.; Xia, W.; Zhang, W. Synthesis and characterization of a novel Zn-Ni and Zn-Ni/Si_3N_4 composite coating by pulse electrodeposition. *Appl. Surf. Sci.* **2018**, *458*, 665−677.

(18) Constantin, I. Microstructural characterization and corrosion behavior of electroless Ni-Zn-P Thin Films. *J. Metal.* **2014**, *2014*, 1−6.

(19) Oriňáková, R.; Turoňová, A.; Kladeková, D.; Gálová, M.; Smith, R. M. Recent developments in the electrodeposition of nickel and some nickel-based alloys. *J. Appl. Electrochem.* **2006**, *36*, 957−972.

(20) Popoola, A. P. I.; Fayomi, O. S. I. Effect of some process variables on zinc coated low carbon steel substrates. *Sci. Res. Essays* **2011**, *6*, 4264−4272.

https://doi.org/10.1021/acsomega.0c01861
ACS Omega 2021, 6, 11139−11143